Selenium passivation of GaAs(001): a combined experimental and theoretical study

2004 J. Phys.: Condens. Matter 16 2187

(http://iopscience.iop.org/0953-8984/16/13/001)

INSTITUTE OF PHYSICS PUBLISHING JOURNAL OF PHYSICS: CONDENSED MATTER

J. Phys.: Condens. Matter **16** (2004) 2187–2206 PII: S0953-8984(04)69670-6

Selenium passivation of GaAs(001): a combined experimental and theoretical study

C González[1], I Benito[1], J Ortega[1], L Jurczyszyn[1,2], J M Blanco[1], R Pérez[1], F Flores[1], T U Kampen[3], D R T Zahn[3] and W Braun[4]

[1] Departamento de Física Teórica de la Materia Condensada, Universidad Autónoma de Madrid, E-28049 Madrid, Spain
[2] Institute of Experimental Physics, University of Wroclaw, pl. M Borna 9, 50-204 Wroclaw, Poland
[3] Institut für Physik, Technische Universität Chemnitz, D-09107 Chemnitz, Germany
[4] BESSY GmbH, Albert-Einstein-Straße 15, D-12489 Berlin, Germany

Received 26 September 2003, in final form 4 February 2004
Published 19 March 2004
Online at stacks.iop.org/JPhysCM/16/2187 (DOI: 10.1088/0953-8984/16/13/001)

Abstract

The chemical and electronic properties of selenium passivated GaAs(001)-2 × 1 surfaces were investigated by a combination of theoretical calculations and core level photoemission experiments. An anion exchange results in gallium-selenide like layers showing a 2 × 1 reconstruction in low energy electron diffraction (LEED). The analysis of the different components in the core level spectra of As 3d, Ga 3d and Se 3d limits the number of possible structural models. The Se/GaAs(001)-2 × 1 reconstruction has been also analysed by means of DFT-LDA calculations and theoretical STM currents. In a first step, different geometries are considered and the most stable one, from the point of view of the thermodynamic potential, is determined. Then, STM currents and the corresponding surface corrugation are calculated and compared with the experimental evidence. We conclude that the Se/GaAs(001)-2 × 1 reconstruction has a single Se atom in the last crystal layer, bonded to two Ga atoms of the second layer, and another Se layer replacing the third As layer of the crystal. These surfaces may be considered as chemically stable because they withstand considerable exposure to air. In terms of electronic passivation, i.e. the removal of any surface band bending, the selenium modification is not successful. Band bending on n-type doped samples is reduced while band bending on the p-type doped samples is further increased.

1. Introduction

The passivation of semiconductor surfaces has two goals, namely chemical and electronic passivation. Chemical passivation means that the surface is inert against the absorption of foreign atoms or molecules. An electronic passivation, on the other hand, should result in a

flat band condition at the surface or, in other words, the Fermi level has the same energy position in the band gap of the semiconductor at the surface and in the bulk. This is achieved by the removal of all surface states within the band gap. Surface states may be charged depending on their character and their energy position with respect to the Fermi level. For example, acceptor type states are negatively charged when they lie below the Fermi level, which is usually the case in n-type semiconductors. This surface charge is compensated by a space-charge layer in the semiconductor, which is connected with band bending. Electronic passivation may be used as a method to control Schottky barrier heights [1]; it has been shown in different theoretical [2] and experimental works [3–6] that passivation tends to reduce barrier heights on n-type doped semiconductors, offering ways of matching barrier heights to device requirements.

Passivation of semiconductors with group VI elements is a well known case for covalent crystals [7, 8]. In particular, when S or Se is deposited on Si or Ge(001) surfaces, the system reacts with the covalent crystal breaking its dimers, and two bonds between the surface atoms and the absorbed species are formed. This reaction has been analysed by many authors who have discussed the degree of surface passivation [9] and its effect on the Schottky barrier height [2].

In the case of As-rich GaAs(001) surfaces, the chalcogen treatment (using S, Se or Te) leads to a gallium-chalcogenide like layer at the surface. Since chalcogen atoms have one excess electron compared to the group V atoms, the dangling bonds of chalcogen surface atoms would be doubly occupied and therefore chemically unreactive. This idea is supported by the results of several experimental investigations. A wet chemical etching of GaAs(001) in sulfide solutions results in an enhancement of the current gain in bipolar transistors [10]. The same treatment increases the optical damage threshold and the slope efficiency of laser diodes [11–13]. On the other hand, a selenium treatment of GaAs(001) surfaces leads to enhanced photoluminescence [14] and to a reduced number of interface states at ZnSe/GaAs heterojunctions [15]. Besides the improved electronic properties of GaAs(001) surfaces and interfaces the chalcogen treatment seems to reduce the chemical reactivity of the surface as well. Thin epitaxial iron films have been grown on sulfur treated GaAs(001) surfaces [16] and sulfur treated Si(001) surfaces serve as substrates for the growth of epitaxial $CuInS_2$ layers [17].

Although all the experimental investigations for both Se and Te on GaAs(001) show the formation of a 2×1 reconstruction in a given temperature range, they disagree on the number of adsorbed chalcogen atoms and on the microscopic structure of the reconstructed surface. In particular, Pashley and Li [18, 19] considered the Se/GaAs(001)case and found, using STM, a well ordered 2×1 reconstruction. The Fermi level on the surfaces of their n-type doped substrates is found to be shifted from a mid-gap position on the unpassivated samples to within 150 meV of the conduction band minimum on the passivated samples. The STM images show that the Se passivation greatly reduces the number of defects on the surface and therefore reduces the pinning of the Fermi level. This reduction in band bending has also been found by Takatani *et al* using photoemisson spectroscopy [20]. In addition, they found that the surface is terminated by a Se layer and As is only in the bulk of the GaAs substrate [20]. With the help of this photoemission data, Pashley and Li proposed a structural model for the Se-passivated GaAs(001) surface, satisfying the electron counting rule [21], with Se located both below the surface replacing As, and also on the surface forming surface dimers. Notice that the additional electrons introduced by the Se atoms require a Ga vacancy at every second site in the fourth layer in order to satisfy the electron counting rule. The schematic ball-and-stick model 4C in figure 1 shows a side view of this structure. Following [22], the nomenclature for the different structures considered in this work (see figure 1) is chosen in such a way that the cipher gives the number of Se atoms in the unit cell and the letter discriminates between configurations with the same number of Se atoms.

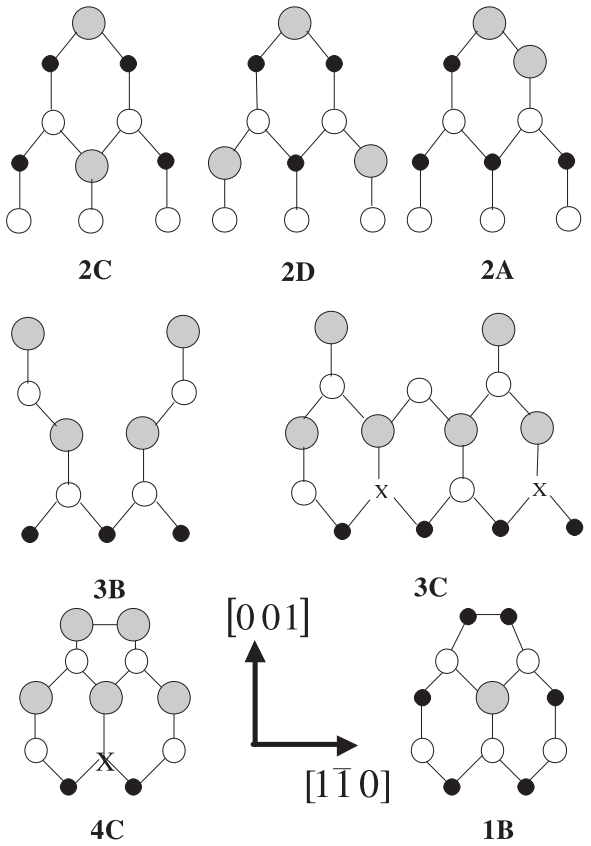

Figure 1. Schematic ball-and-stick models of the structures considered in this work for the Se/GaAs(001) 2 × 1 reconstruction. The cipher in the label corresponds to the number of selenium atoms per unit cell, while the letter discriminates between configurations with the same number of Se atoms. Grey circles correspond to Se atoms, white circles to Ga atoms and black circles to As atoms. The X indicates Ga vacancies that are introduced in some of the models to fulfil the electron counting rule.

Gundel and Faschinger [22] have studied theoretically the cases of Se or Te on GaAs(001) using first-principles simulations. They considered 11 different structures that satisfy the experimentally observed 2 × 1 reconstruction and the electron counting rule (see figure 2 in [22]). The total energy for each of these structures was determined by DFT-LDA calculations. Since the amount of adsorbed chalcogen atoms per 2 × 1 surface cell varies in the different structures, it is necessary to account for the effects of the varying stoichiometry when comparing the relative stability of the different structures. They determined the corresponding thermodynamic surface potential as a function of the different chemical potentials and concluded that the structures 1A (with a mixed As–Se surface dimer), 3B and 6A (both with no Se surface dimers, see our figure 1 and figure 2 in [22]) are among the most stable ones, while the 4C structure proposed by Pashley and Li [18, 19] is one of the less energetically favourable structures.

Considering the discussion above, the question arises as to how the apparent instability of the Se dimer 4C structure can be made congruent with the experimental evidence of [18, 19]. As already recognized by Gundel and Faschinger, and discussed in section 4 below, total

energy calculations suggest a candidate structure with the lowest surface energy, but the question of the real microscopic structure cannot be decided from them alone [22]. Detailed photoemission experiments that restrict the number of models valid to describe the passivated surface, and the theoretical simulation of the STM data of Pashley and Li [18] provide the crucial complementary evidence needed to determine the correct model for this passivated surface.

In this paper we present the combined experimental and theoretical study needed to determine the microscopic structure of the Se/GaAs(001)-2 × 1 surface. Soft x-ray photoemission spectroscopy is used to investigate the chemical and electronic properties of selenium modified GaAs(001) surfaces. Section 2 describes the experimental details. Section 3.1 presents the core level spectra of samples prepared by two different preparation procedures. Both procedures result in surfaces with the same chemical surface composition and structure, but with slightly different efficiency. The analysis of the components in the As 3d, Ga 3d and Se 3d core level spectra provides evidence for the number of inequivalent chemical environments for these atoms and reduces the number of possible structural models. The electronic properties of these surfaces are presented in section 3.2. Here, the emphasis is on the position of the Fermi level on Se-passivated GaAs(001) surfaces for n- as well as p-type doping. Electronic passivation will be achieved when the Fermi level assumes the same position at the surface as in the bulk, that is the surfaces show no surface band bending. In most studies on the electronic properties of passivated GaAs(001) surfaces only n-type doped substrates have been used. It is tempting to conclude that the often observed reduction in surface band bending on n-type doped GaAs(001) surfaces induced by Se passivation will also be achieved on p-type doped GaAs(001) substrates. But our investigations on n- and p-type doped samples prepared and investigated under identical conditions will show that this is not the case.

Our theoretical approach combines both density functional theory (DFT) total energy calculations (section 4) and simulations of the STM images (section 5) for different structures (see figure 1). We have explored the stability of a few other structures not considered in previous studies. All these structures have in common the presence of a single Se atom instead of the Se dimer postulated by Pashley and Li [18] in the top layer of the reconstruction. This choice is based on the theoretical analysis of the experimental STM images afforded by these researchers that, as shown below (section 5), are typical of a single Se atom geometry. Figure 1 shows the new structures (2C, 2D and 3C), together with two structures with a single Se atom on the top layer (2A and 3B) already discussed by Gundel and Faschinger [22]. In the same figure we also include structures with an As dimer (1B) and a Se dimer (4C, the original Pashley model) that are relevant for our discussion of the STM images. The combination of the experimental and theoretical evidence presented in this paper, summarized in section 6, shows that the structure 3B (see figures 1 and 2) represents the appropriate atomic geometry for the Se passivated GaAs(001)-2 × 1 reconstruction.

2. Experimental details

Homoepitaxial n- and p-type GaAs(001) layers with a doping concentration of $N = P = 1 \times 10^{18}$ cm^{-3} served as substrates in this study. After their growth by molecular beam epitaxy they were covered by a thick amorphous arsenic layers to protect the GaAs(001) surfaces against contamination and oxidation. These samples were transferred into an ultra-high vacuum system with a base pressure of $p < 2 \times 10^{-10}$ mbar. The arsenic layer was then removed by gentle annealing to 380 °C. This leads to an As-rich c(4 × 4) surface reconstruction of the GaAs(001) surface as can be judged from the lineshape analysis of

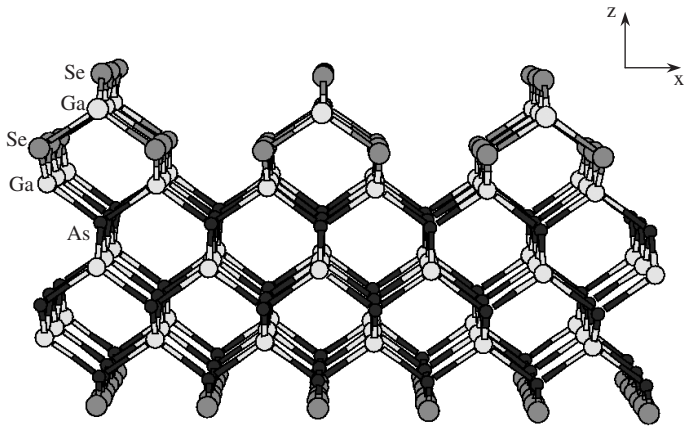

Figure 2. Lateral view of structure 3B in figure 1. z and x correspond to the [001] and [1$\bar{1}$0] crystallographic directions. Notice the presence of Se chains (each Se atom is bonded to two of the Ga atoms below) in the [110] direction.

the measured photoemission spectra and additional LEED experiments. For the selenium passivation the compound $SnSe_2$ was used as source material [23]. This compound decomposes at high temperatures according to

$$SnSe_2 \longrightarrow SnSe + Se\uparrow \qquad \text{at } 340\,^{\circ}\text{C}\,. \tag{1}$$

A Knudsen cell like oven equipped with Ni–Ni/Cr thermocouples was used for the deposition of selenium. The deposition rate is monitored by a quartz crystal microbalance and controlled by the current from a stabilized power supply. The substrates were either kept at room temperature (RT) or elevated temperature. In the first case several selenium deposition steps followed by annealing of the sample at 480 °C were performed. In the later case Se was evaporated on the substrate held at elevated temperatures around 350 °C.

The photoemission measurements were performed at the TGM 2 beamline of the synchrotron radiation source BESSY at Berlin. The UHV chamber at this beamline is equipped with a VG ADES 400 electron spectrometer providing a combined resolution of both light and photoelectrons of about 300 meV at 65 eV photon energy. The photon energy was varied so that the Ga 3d, As 3d, and Se 3d core levels were each recorded at a kinetic energy of approximately 50 eV. At this kinetic energy the electrons have a minimum escape depth. Therefore, maximum surface sensitivity is achieved. The width of a core level line is determined by many factors: the intrinsic lifetime of the core hole, the instrumental resolution, the presence of satellites, and disorder and potential variations across the surface which result in inhomogeneous band bending of the surface [25, 26]. The spectra were decomposed by curve fitting using Voigt functions, a Lorentzian convoluted with a Gaussian lineshape, for the different components and a Shirley background applying a method presented by Joyce [24]. When a core level line is curve fitted using a Voigt function, the broadening in the Lorentzian shape results from the lifetime of the core hole, while the Gaussian broadening accounts for the instrumental resolution and also for any broadening due to the sample conditions. The Lorentzian line widths were kept constant during the fitting procedure, while intensities, binding energies and Gaussian line widths were variable. The parameters kept constant are listed in table 1 and agree well with the values evaluated by others [27–29, 31]. The Gaussian line widths for the Ga 3d, As 3d and Se 3d core level emission were in the range of 0.4, 0.5 and 0.8 eV, respectively. Compared to the experimental resolution the Gaussian broadening is larger, which can be

Table 1. Fit parameters for the core levels, which were held constant during the fitting procedure.

	Ga 3d	As 3d	Se 3d
Lorentzian width (eV)	0.1	0.1	0.1
Branching ratio	1.68	1.5	1.5
Spin–orbit splitting (eV)	0.44	0.69	0.86

Table 2. Binding energies and binding energy shifts of the different components in the photoemission spectra of the As $3d_{5/2}$, Ga $3d_{5/2}$ and Se $3d_{5/2}$ core levels for the clean and the Se-passivated GaAs(001) surfaces grown on n- and p-type substrates. Passivated surfaces are modified by selenium atoms at elevated temperatures.

		E^{n}_{Bin} (eV)	E^{p}_{Bin} (eV)
GaAs(001)-c(4 × 4)	Ga1	19.26 ± 0.07	19.10 ± 0.07
	Ga2	+0.46 ± 0.12	+0.48 ± 0.13
	As1	41.14 ± 0.08	40.98 ± 0.12
	As2	+0.62 ± 0.03	+0.65 ± 0.04
	As3	−0.50 ± 0.04	−0.48 ± 0.07
GaAs(001):Se-2 × 1	Ga1	19.57 ± 0.08	19.24 ± 0.04
	Ga3	+0.37 ± 0.04	+0.39 ± 0.04
	Ga4	+1.07 ± 0.04	+1.07 ± 0.04
	As1	41.38 ± 0.09	41.14 ± 0.08
	As4	+1.3 ± 0.04	+1.3 ± 0.04
	Se1	54.6 ± 0.1	54.1 ± 0.1
	Se2	+0.92 ± 0.04	+0.93 ± 0.03

attributed to a lateral variation of surface band bending, that is inhomogeneous surface band bending.

The Fermi level position at the clean GaAs surface was determined by carefully measuring the distance between the Fermi edge of the metal sample holder and the valence band maximum (VBM). Changes in the Fermi level position after each modification step were followed by determining the change in the energy position in the bulk components of the Ga 3d and As 3d core level emission. The binding energies of all core level components for n- and p-type substrates are listed in table 2.

3. Photoemission spectroscopy studies

3.1. Se modified GaAs(001) surfaces

The As 3d and Ga 3d core level emission spectra of the GaAs(001)-c(4 × 4) surface are shown in figure 3(a). After decapping the protecting As layer, the As 3d consists of three components. The As1 component is attributed to As in the fourfold coordinated environment of the GaAs bulk. The components As2 and As3 are shifted by 0.62±0.03 and 0.50±0.04 eV towards higher and lower binding energy, respectively. The higher binding energy component originates from As atoms in the surface dimers in the first layer of the As-rich GaAs(001) surface [31, 32]. The As3 component is attributed to threefold coordinated As atoms in the second As layer of the sample. The Ga 3d core level presents two components: a bulk component (Ga1) and a surface component (Ga2), which is shifted by 0.46 eV towards higher binding energies and is attributed to Ga atoms below the threefold coordinated As atoms [31].

The As 3d, Ga 3d and Se 3d core levels of a GaAs(001) surface prepared by Se evaporation followed by annealing are shown in figure 3(b). Here, usually two cycles of

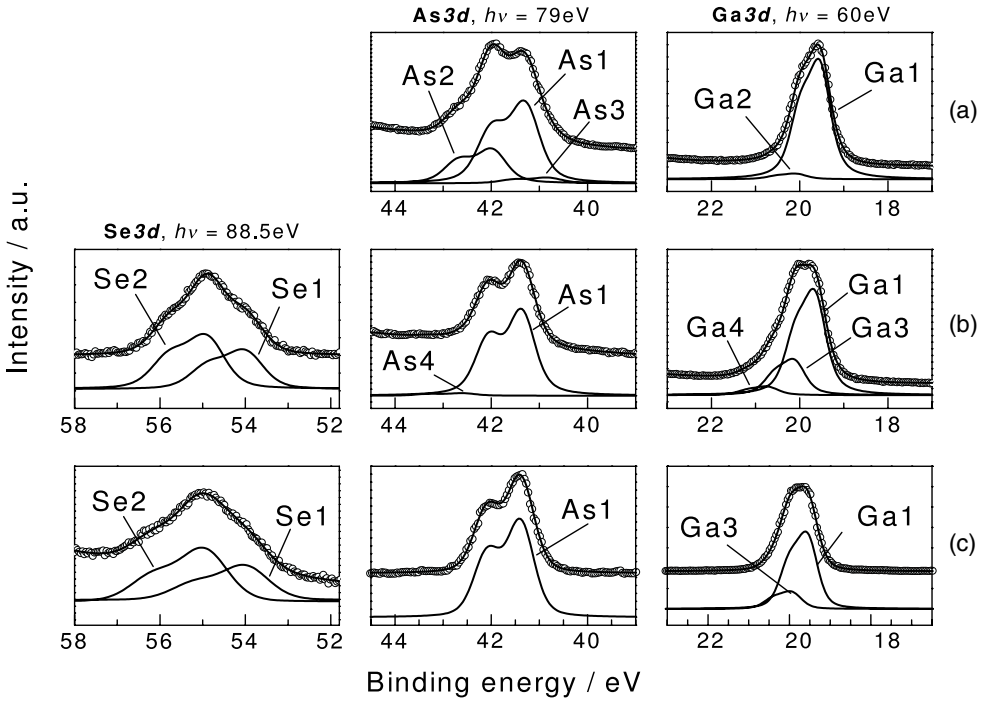

Figure 3. Se 3d, As 3d and Ga 3d core level spectra (a) of the clean c(4 × 4) reconstructed GaAs(001) surface after decapping, (b) after evaporation of Se followed by annealing at 480 °C, and (c) after Se evaporation on a substrate held at an elevated temperature (around 350 °C).

Se evaporation (∼30 nm) and annealing were sufficient to obtain stable surface properties. In the As 3d core level spectra the As2 and As3 components disappear and a new component As4 on the higher binding energy side is observed. This component is shifted by +1.3 eV with respect to the bulk component As1 and is a result of the formation of As_2Se_3 at the surface [20, 35, 36]. This reaction takes place between the excess As on the As-rich GaAs(001) surface and the deposited Se and is energetically favoured because of its heat of formation of -97 kJ mol^{-1} [33], which is larger than the heat of formation of GaAs (-71 kJ mol^{-1}) [34]. Annealing to 380 °C removes nearly all the arsenic selenide [20, 35] on the sample surface, resulting in a dominant As bulk component in the As 3d spectrum. In the Ga 3d spectrum in figure 3(b) the Ga2 component disappears and two new Ga components, Ga3 and Ga4, shifted in binding energy by 0.37 and 1.07 eV, respectively, can be identified. The Ga3 component is attributed to Ga bonded to Se on the surface and is in good agreement with data already published in the literature [37]. The Ga4 component, on the other hand, is attribute to subsurface Ga at the interface between the Se modified surface and the GaAs bulk. For the Se 3d two different components can be observed, which are separated by 0.92 eV. The two Se components Se1 and Se2 are attributed to surface and subsurface components, respectively, and the energy difference as well as the intensity ratio Se1/Se2 of 1.37 coincides quite well with the values published by Takatani *et al* [20] and Märkl *et al* [38].

Photoemission spectra for a GaAs(001) surface where the Se treatment has been performed at elevated sample temperatures are shown in figure 3(c). Comparing the spectrum of the As 3d displayed in figure 3(c) with the one displayed in figure 3(b) shows that the As4 component does not occur in the latter. The Ga 3d in figure 3(b) shows, besides the bulk component,

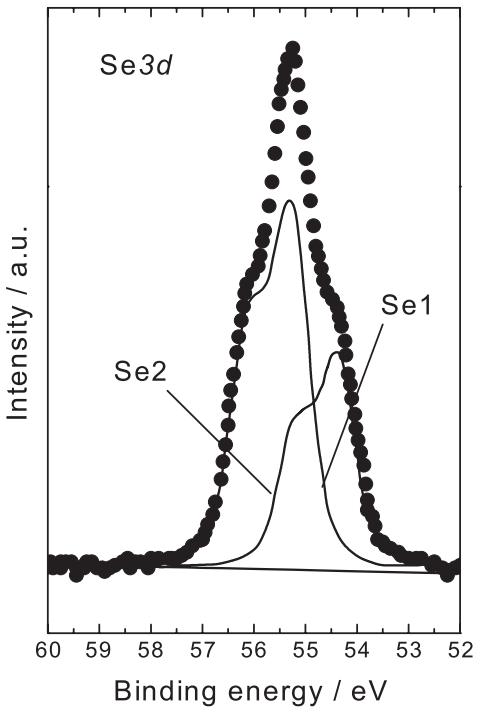

Figure 4. Se 3d core level emission recorded from Ga_2Se_3 layers grown on GaAs(001) using a heterovalent exchange reaction.

only the component Ga3. The disappearance of both components As4 and Ga4 indicates the formation of an abrupt interface between the Se-modified surface and the GaAs bulk. This is due to a more efficient As/Se exchange reaction and As_2Se_3 desorption for the Se deposition at high temperatures. Photoemission spectra of the Se 3d core level of the Se modified GaAs(001) surface at elevated temperatures (figure 3(c)) only differ from the spectra displayed in figure 3(b) by a slightly higher binding energy difference of 0.92 eV between the two Se components. It should be mentioned that both passivation procedures show a 2×1-reconstructed surface in LEED, the surfaces prepared at elevated temperatures showing sharper LEED spots. This 2×1 reconstruction has also been observed by others for the Se-modified GaAs(001)surface [20, 39–41].

The additional component Ga3 and the Se 3d core level spectra indicate the formation of a Ga_2Se_3 terminated surface. In the case of GaSe, the Ga 3d and Se 3d core level spectra would show only one component each [30]. In addition, the Se 3d core level spectra in figure 3 will now be compared with Se 3d core level spectra recorded at a surface of Ga_2Se_3. Figure 4 shows the Se 3d core level emission recorded from Ga_2Se_3 layers grown on GaAs(001) using a heterovalent exchange reaction. The overall shape of the Se 3d core level spectrum is the same as for the one taken from the Se-passivated surfaces. Two components are observed which are separated by 1 eV with the one at higher binding energy having the higher intensity. This is in agreement with Se 3d core level spectra taken from the passivated GaAs(001) surface and shows that the composition of the passivated surfaces is Ga_2Se_3 like.

The formation of a Ga_2Se_3 like surface layer is also evident from the As 3d to Ga 3d intensity ratio $I_{As\,3d}/I_{Ga\,3d}$ determined from spectra excited with a photon energy of 88 eV. For

the clean c(4 × 4) reconstructed GaAs(001) surface, which is As-rich, $I_{As\,3d}/I_{Ga\,3d}$ is determined to be about 1.3. On the Se-passivated GaAs(001) surface $I_{As\,3d}/I_{Ga\,3d}$ is reduced to 0.6, clearly indicating the loss of As in the surface region. Again, these intensity ratios are in agreement with the data published by Takatani *et al* [20].

In conclusion, it can be said that the core level spectra shown here represent a unique fingerprint of the Se-passivated GaAs(001) surface. The core level spectra will now be used to determine the possible structure model, which describes the Se-passivated GaAs(001) surface. From the experimental data it can be concluded that As exists only in the bulk of GaAs and has no surface component. This result reduces the number of possible structural models for the description of the Se passivated GaAs(001) to models 3B, 3C and 4C. In 3C, Ga will be found in four different chemical environments, while in 3B and 4C the chemical environment of Ga is the same, resulting in three core levels, in agreement with the experimental results. Here, one finds Ga bonded to four As atoms, Ga bonded to two As and two Se atoms, and Ga atoms bonded to four Se atoms. The chemical environment for the Se atoms is also similar, i.e. Se is found in two different bonding configurations. Therefore, it is not possible to discriminate between the two different structural models 3B and 4C by just considering the core level shifts. The results from the theoretical calculations in sections 4 and 5 will provide further information to determine the most appropriate geometry of the Se passivated GaAs(001) surface.

The chemical stability and unreactivity of the selenium treated surface is evidenced by the fact that the 2 × 1 reconstruction of the surfaces can be observed after exposing the samples to air for a few minutes and then transferring them back into UHV.

3.2. Electronic properties

Dangling bonds, surface defects or adatoms on semiconductor surfaces generally induce changes in surface band bending. This effect is caused by surface states induced by the above mentioned effects and the surface band bending involves charge transfer from these surface states into an extended space-charge layer beneath the surface. Occupied or non-occupied surface states of acceptor character are negatively charged or neutral, respectively. Therefore, only acceptor surface states below the Fermi level are charged negatively and are most probably detected on n-type semiconductor surfaces, where the Fermi level is close to the conduction band minimum under flat band conditions. The charge in acceptor surface states is compensated by a space charge of positive sign. This is achieved by an upward bending of the bands at the surface resulting in a region being depleted of electrons. The space charge is carried by the now uncompensated positively charged bulk donors. For surface states of donor type character the situation is reversed. Here, donor type surface states are positively charged above the Fermi level and will result in band bending on p-type semiconductor surfaces. Already concentrations of surface states well below 1% of a monolayer will lead to what is called a *pinning of the Fermi level* on semiconductor surfaces. Such a Fermi level pinning and its associated band bending may persist in devices prepared on such semiconductor surfaces resulting in injection barriers for charge carriers at semiconductor interfaces. To avoid these problems special surface treatments are used to achieve what is called a surface electronic passivation. A detailed description of the properties of semiconductor surfaces and interfaces can be found in the monographs written by Lüth [42] and Mönch [43]. In this section we explore, following the evolution of the Fermi level on p- and n-type doped samples, the efficiency of the Se treatment for the electronic passivation of the surface.

For the as-received surfaces the Fermi level is determined to be 0.5 and 0.63 eV above the VBM for the sample doped p- and n-type, respectively. After removing the As cap by annealing, the Fermi level is found to be shifted closer to the VBM. The energy positions

are 0.42 and 0.6 eV for the sample doped p- and n-type, respectively. The evolution of the Fermi level position is then monitored by the binding energy shifts of the Ga 3d and As 3d bulk components with respect to the corresponding values of the clean surface. After the Se treatment, the Fermi level moves closer to the conduction band minimum, the energy positions relative to the VBM being 0.55 and 0.9 eV for the sample doped p- and n-type, respectively. This indicates a decrease (increase) of band bending on samples doped n-type (p-type). Thus, while n-type samples show some hint of a successful passivation, the p-type ones still show strong band bending. The reduction in band bending on n-type doped substrates agrees well with experimental results obtained by Pashley and Li [18, 19]. In the p-type case, our experimental results clearly disagree with the band bending reduction guessed (they only measured n-type samples) by Pashley and Li.

The residual band bending for both types of doping can be due to the intrinsic properties of the Se-passivated surface and/or to surface defects. Since a band bending is detected for both types of doping, surface states of donor as well as acceptor type character are present in the band gap of the semiconductor. Therefore, a Se treatment leads to new electron surface states within the band gap. From the STM study of Pashley and Li [18, 19] it is known that even a very well ordered Se terminated 2×1 surface shows two types of defect: a few small holes simply from 'missing dimers' and many more small bright features. The density of these bright features is approximately 1×10^{12} cm^{-2} in the image, which matches the density of dopant atoms on the surface at the doping concentration of (3–6) $\times 10^{18}$ cm^{-3} used in their study. The doping level of the GaAs substrates used in our experiments is almost the same, therefore the number of dopant atoms on the surface would also be 1×10^{12} cm^{-2} among 6×10^{14} cm^{-2} surface atoms. This means there is approximately one dopant atom in 300 surface unit cells. This density of defects at the surface is enough to significantly influence the position of the Fermi level within the band gap of the semiconductor.

4. DFT-LDA calculations

We have used a first-principles local-orbital code [44] (FIREBALL96) to perform energy minimization calculations of the structures shown in figure 1. Norm-conserving pseudopotentials [45] are used to simulate the ion cores and a DFT approach to model the valence electrons. Exchange and correlation energy contributions are introduced by the local density approximation (LDA) [46]. As, Ga and Se wavefunctions are described with a minimal basis, including s and p atomic like FIREBALL orbitals with cutoff radius of 5.0, 5.2 and 4.6 au, respectively. These values provide similar energy shifts for the orbital levels in those confined atoms (compared to the orbitals in the free atom) and thus ensure that the atomic electronegativities are preserved.

We have employed a supercell approach, considering an asymmetric slab of atoms containing 10 atomic layers with a 2×1 surface periodicity (see figure 2). The bottom of the slab is an As-terminated unreconstructed GaAs(001) surface, where the dangling bonds are passivated with hydrogen like pseudoatoms with a nuclear charge of $Z = 0.75$ and the corresponding valence charge. Being a local-orbital real-space method, the periodicity in the direction perpendicular to the surface can be chosen to ensure that the vacuum between adjacent slabs is large enough (>50 Å) to make interactions completely negligible. All the atoms, apart from the ones in the last two bottom layers that are kept fixed at their bulk positions, are fully relaxed to determine the ground state. The evolution of both the total energy and the atomic displacements is used to monitor the relaxation. The process is stopped when the changes are less than 10^{-6} eV/atom and 0.02 Å respectively. 64 special **k** points, generated with the

Monkhorst and Pack scheme [47], have been used to sample the first Brillouin zone. The performance of the code has been extensively checked in a number of systems against fully converged plane-wave DFT calculations (see, for example, [48, 49]).

As we have to compare surface structures with different chemical compositions, it is necessary to account for the effects of varying stoichiometries properly. We have followed the same approach of Gundel and Faschinger [22]. The adsorbate-covered surfaces are assumed to be in thermal equilibrium, being able to exchange individual atoms of their constituents from appropriate reservoirs. The appropriate thermodynamical potential (called surface energy in [22]), Γ is then given by:

$$\Gamma = E_{\text{tot}} - \sum_i \mu_i N_i \tag{2}$$

where E_{tot} denotes the total energy for one supercell obtained in the simulation and μ_i and N_i the chemical potential and number of atoms of constituent i, respectively, within the supercell. Certain boundary conditions and relations among the chemical potentials for the different constituents can be established from thermodynamic equilibrium considerations (e.g. the chemical potential at the surface is equal to the value for the bulk beneath) and total energy calculations (e.g. the lower limit of μ_{As} can be fixed by the heat of formation of GaAs, ΔH_{f}^0(GaAs)). In this way, surface energies can be calculated as a function of the differences between the chemical potentials of As and Se and their respective bulk values (see [22] for details).

Our calculations for the structures considered by Gundel and Faschinger reproduce their surface energy results (see figure 3 in [22]) within an accuracy of ± 0.3 eV per 2×1 surface unit cell. In particular, we also find that the 3B structure (see figure 2 for a perspective of the relaxed geometry) is the most stable one for a large range of chemical potentials (except for $\mu_{\text{As}} = \mu_{\text{As}}^{\text{bulk}} - \Delta H_{\text{f}}^0$ (GaAs) and $\mu_{\text{Se}} \cong \mu_{\text{Se}}^{\text{bulk}} \leqslant -1.8$ eV, and $\mu_{\text{As}} = \mu_{\text{As}}^{\text{bulk}}$ and $\mu_{\text{Se}} \cong \mu_{\text{Se}}^{\text{bulk}} \leqslant -1.1$ eV). The detailed comparison between our results and those of [22] can be illustrated precisely for the chemical potentials around $\mu_{\text{As}} = \mu_{\text{As}}^{\text{bulk}} - \Delta H_{\text{f}}^0$(GaAs) and $\mu_{\text{Se}} - \mu_{\text{Se}}^{\text{bulk}} = -1.8$ eV where the stability crossing between the 3B and other structures takes place. At that value, we have found that $\Gamma(3\text{B}) \simeq \Gamma(1\text{B}) \simeq \Gamma(1\text{A})$, at variance with [22] where structure 1A is approximately 0.3 eV lower in energy than 3B and 1B. Structures 1C and 2A are 0.50 and 1.2 eV higher in energy than the 3B structure at that point (compared to 0.25 and 1.37 eV in [22]).

We have also studied the energetics of new structures, like models 2C, 2D and 3C, that all have in common the presence of a single Se atom (not a dimer) on the surface. Structures 2C and 2D have a very similar energy to the structure 2A considered in [22]. Notice that all of these structures have the same stoichiometry with Se atoms replacing As at different sites. The structure 3C can be obtained from the case 3B, by moving a Ga atom from the fourth to the second layer. According to our calculations, creating the fourth-layer Ga vacancy is too expensive, with the structure 3C being energetically less favourable than the structure 3B by 4.0 eV per 2×1 surface unit cell. We conclude that, from the thermodynamical point of view, the 3B model is the most likely structure for the Se-passivated surface.

Figure 5 shows the electronic band structure of the relaxed 3B geometry. The first thing to comment on is the good passivation this geometry shows, with an energy gap of $\sim$2 eV, very close to the energy gap calculated for bulk GaAs. Notice that, in our minimal basis set calculations, the conduction band is not very well reproduced, giving an overestimation of a few tenths of eV with respect to the experimental GaAs gap. Figure 6 shows the local density of states (LDOS) associated with different atoms. This LDOS has been calculated using Green function techniques, where the imaginary part of 0.1 eV in the energy, $\omega + 0.1\imath$, introduces a small broadening in the states.

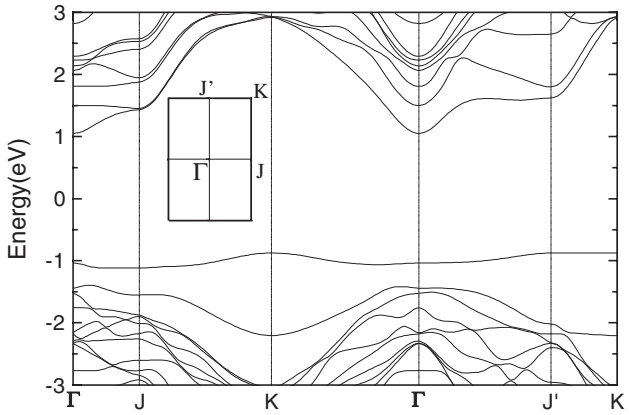

Figure 5. Surface bands for structure 3B in figure 1. The zero of energy corresponds to a position close to the middle of the GaAs semiconductor gap.

Comparing figures 6 and 5, we see that the top-most valence band is associated with the surface Se atom, while the bottom-most conduction band is associated with the bonds formed between the Se and Ga atoms of the third and fourth crystal layers. Figure 6 also shows the different contributions associated with the s and p orbitals in the LDOS of the topmost Se atom. From this figure, we deduce the p_x character of the topmost valence band (the x-direction is indicated in figure 2). The small dispersion of this band is the result of the large distances, around 4.0 Å, between the Se nearest neighbours in the y direction and the π character of the interaction between these p_x orbitals. The second occupied valence band, that lies within the upper bulk GaAs valence bands, has p_z character, and it is responsible for the broader peak between -2.5 and -1.5 eV in the Se surface atom LDOS. In the next section we shall relate this electronic structure to the STM images.

According to our total energy calculations for the different structures (including the new ones shown in figure 1), the 3B geometry (already found by Gundel and Faschinger [22] as one of the most stable structures) seems to be the best candidate to represent the Se-passivated GaAs(001). We should say at this point that DFT-LDA calculations show some uncertainties related to the values of the chemical potentials used to calculate the surface thermodynamic potential. While the DFT-LDA approximation provides a good description of the structural properties (related to *energy variations* around the total energy minimum), it usually overestimates the absolute value of the total energy associated to that minimum. This implies that while we can be sure about the quality of the ground state obtained through the energy minimization of the different structures considered, we are less confident about the absolute values for the total energy. When the comparison is possible, our results reflect this well-known limitation: our calculated chemical potentials for Ga, As and Se are larger (more negative) by around 2 eV than the experimental values. The comparison between the different structures involves the comparison of absolute values of the surface thermodynamical potential (combining the total energy of each structure and the contribution associated to the different stoichiometry through the chemical potentials), and our results show that these differences are small and that the relative ordering can be quite sensitive to the values of the chemical potentials. Thus, the relative stability extracted from DFT-LDA calculations should be taken only as indicative of the most favourable structure, and this total energy analysis should be complemented by other independent evidence to assess the validity of the structural model obtained in this way.

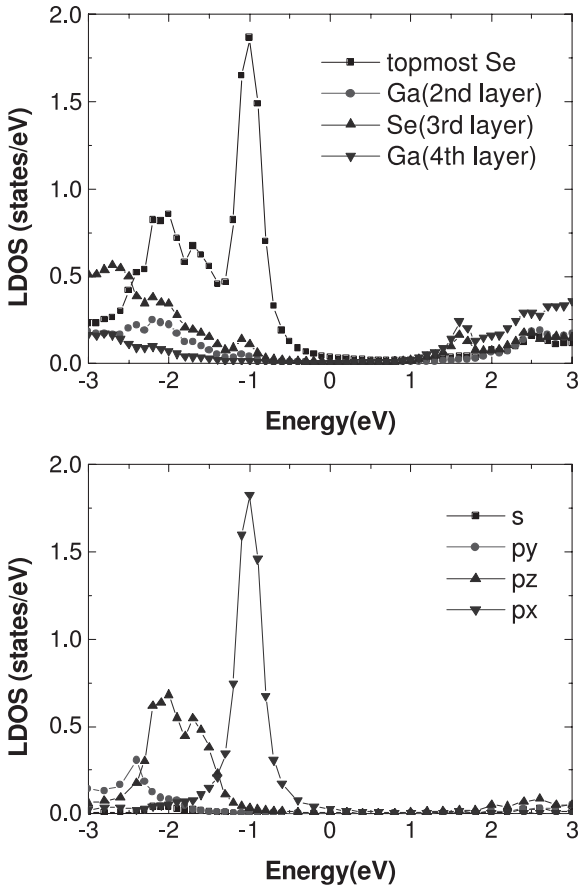

Figure 6. LDOS for the atoms in the last four layers of the 3B structure (top). The projection on the different orbitals is shown for the topmost Se atoms (bottom). Energy zero as in figure 5. Notice that there is an additional broadening due to the imaginary part of 0.1 eV that has been included in the calculation of the LDOS using Green function techniques.

Theoretical simulations of the STM images for different structures (including the Se dimer model of Pashley and Li) and their comparison with the experimental STM images, discussed in the next section, provides the complementary information necessary to validate the 3B structure as the correct model for the passivated surface.

5. STM images

Tunnelling currents between an STM tip and the substrate can be calculated using a non-equilibrium Keldysh–Green function approach formulated in terms of a linear-combination-of-atomic-orbitals (LCAO) Hamiltonian [50]. While originally formulated in terms of parametrized tight-binding Hamiltonians, this formalism can be naturally linked with the DFT-LDA calculations in the local orbital basis discussed above, using the Hamiltonian obtained from the FIREBALL96 code to provide first-principles calculations of the STM currents [51].

In this local orbital approach, we describe the tunnelling currents by means of the following Hamiltonian:

$$\hat{H} = \hat{H}_{\mathrm{T}} + \hat{H}_{\mathrm{S}} + \hat{H}_{\mathrm{I}}, \tag{3}$$

where the sample Hamiltonian $\hat{H}_S$ is obtained[5] from the FIREBALL96 calculations, $\hat{H}_T$ is the tip Hamiltonian and $\hat{H}_I$ describes the tip–sample coupling (see [50, 51] for further details). Assuming $\hat{H}$ to be known, the tunnelling current is given, to all orders in the coupling, by:

$$J = \frac{4\pi e}{\hbar} \int_{-\infty}^{\infty} \mathrm{Tr}\left[T_{ts}\rho_{ss}(\omega) D^{R}_{ss}(\omega) T_{st}\rho_{tt}(\omega) D^{A}_{tt}(\omega)\right] [f_t(\omega) - f_s(\omega)]\, \mathrm{d}\omega \tag{4}$$

where

$$D^{R}_{ss}(\omega) = \left[I - T_{st} g^{R}_{tt}(\omega) T_{ts} g^{R}_{ss}(\omega)\right]^{-1} \tag{5}$$

$$D^{A}_{tt}(\omega) = \left[I - T_{ts} g^{A}_{ss}(\omega) T_{st} g^{A}_{tt}(\omega)\right]^{-1}. \tag{6}$$

In equation (4) ρ_{ss} and ρ_{tt} are the density matrices associated with the sample and the tip, respectively; T_{ts} is the hopping matrix defining the tip–sample interaction and $\hat{I}$ is the unit matrix. $g^{R}_{tt}(\omega)$ and $g^{A}_{ss}(\omega)$ are the tip and sample Green functions (A = advanced, R = retarded), while $f_t(\omega)$ and $f_s(\omega)$ define the tip and sample Fermi distribution functions. Notice that all the dependence of J with the tip–sample distance enters into that expression through the distance variation of the tip–sample hoppings T_{ts}. For zero temperature and a bias V, equation (4) yields:

$$J = \frac{4\pi e}{\hbar} \int_{0}^{eV} \mathrm{Tr}\left[T_{ts}\rho_{ss}(\omega) D^{R}_{ss}(\omega) T_{st}\rho_{tt}(\omega) D^{A}_{tt}(\omega)\right] \mathrm{d}\omega. \tag{7}$$

For large distances between the tip and the sample, where most of the STM experiments are performed, $\hat{D}^{R}$ and $\hat{D}^{A}$ can be replaced by the identity matrix, and

$$J = \frac{4\pi e}{\hbar} \int_{0}^{eV} \mathrm{Tr}\left[T_{ts}\rho_{ss}(\omega) T_{st}\rho_{tt}(\omega)\right] \mathrm{d}\omega \tag{8}$$

with the tunnelling current given by the sample and tip density matrices and the tip–sample interaction.

In our approach ρ_{ss} is obtained from the FIREBALL96 calculations in the way described above. The W tip is represented by a four atom pyramidal cluster (with a single atom at the cluster apex), with the influence of the rest of the tip simulated by Bethe lattices connected to the three atoms of the cluster second layer [52]. From this model we calculate the ρ_{tt} that we insert in equation (8). We should also mention that, for the tip, we did not perform any DFT-LDA calculation; we take the first nn interactions given by [53] for W and modify the corresponding diagonal levels to obtain local neutrality charge conditions. This will be enough for having a qualitative description of the tip electronic structure; a more refined calculation would be only justified if we had a better knowledge of the tip geometry.

Finally, the hopping interactions, T_{ts}, have been calculated in two different ways. In one case, we have used the following equation:

$$T_{ij} = -(\gamma/2) \int_{S_{ij}} (\psi_i \vec{\nabla} \psi_j - \psi_j \vec{\nabla} \psi_i) \cdot \vec{n}\, \mathrm{d}s, \tag{9}$$

where ψ_i and ψ_j are the atomic orbitals under consideration and γ is a coefficient that typically takes values in the range 1.3–1.5 (see [54]). In the second case, T_{ij} has been calculated considering the dimer formed between the atoms where the orbitals i and j are located. A quantum chemistry program provides the matrix elements, T_{ij}, we are interested in. In the calculations presented below, both approaches for calculating T_{ij} were used, without significant differences between their results.

[5] $\hat{H}_S$ is written in an orthonormal basis, obtained from the atomic like FIREBALL orbitals by means of a Löwdin transformation.

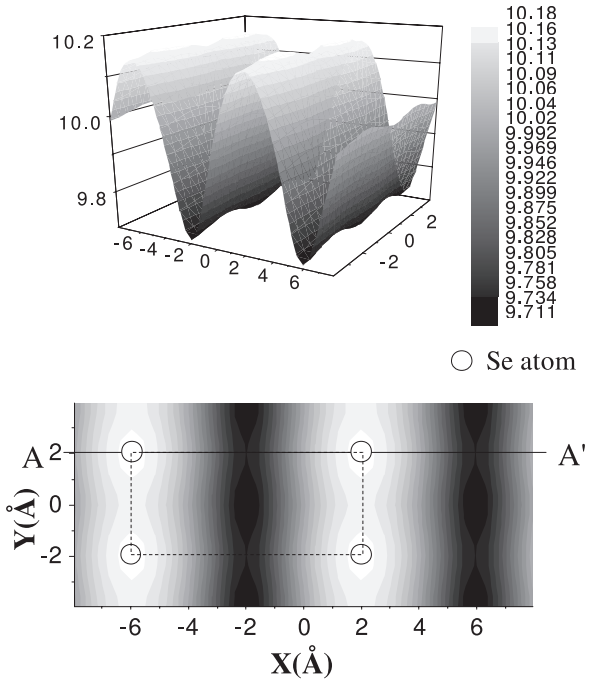

Figure 7. Topographical (constant current) STM image (3 V, 0.1 nA) for the 3B structure. X and Y correspond to the $[1\bar{1}0]$ and [110] crystallographic directions (see figures 1 and 2). The scales in X, Y and Z directions are in Å. The reference point at $z = 0$ corresponds to the height of the Se atoms. The rectangle (dashed line) corresponds to the surface unit cell and white circles indicate the position of the Se atoms. The spacing between the contour lines is 0.0235 Å.

A word of caution should be put here because, in principle, calculating T_{ij} from equation (9) with the FIREBALL local orbitals used in our total energy calculations would be inappropriate. The reason is the cutoff radius one has introduced in these local orbitals within the FIREBALL code [44]. This makes T_{ij} zero for the tip–sample distances we have to consider to simulate the experiments (see below). Then, we have calculated T_{ij} using atomic orbitals having the right long-distance behaviour. We stress, however, that in our calculations for J (equation (8)), ρ_{ss} is determined from the Hamiltonian obtained from the DFT-LDA calculation with the FIREBALL96 code, where the relevant short-distance behaviour of the atomic wavefunctions is properly included and, thus, the electronic band structure is well described. A detailed discussion of the accuracy of this combined approach for the calculation of the tunnelling currents will be published elsewhere [55].

Using this approach we have calculated the tunnelling currents. Figure 7 shows the STM topography of the 3B structure as calculated for $V = 3.0$ eV and $I = 0.1$ nA, in the constant current mode. A detailed surface topography scan along the AA′ line of figure 7 can be found in figure 8. The differential conductance, $\mathrm{d}I/\mathrm{d}V$, as a function of the applied bias, V, on top of one of the Se atoms is displayed in figure 9. In these last two figures, the experimental data taken from [18], for the topography scan and the differential conductance respectively, is included.

All these calculations compare well with the date of Pashley and Li; first, the STM topography of figure 7 is in good agreement with the topography given by those authors (see also figure 3(b) in [18]). Moreover, the average experimental corrugation (where the noise in the data is eliminated) of around 0.70 Å (see figure 3(c), curve (ii), of [18]) compares

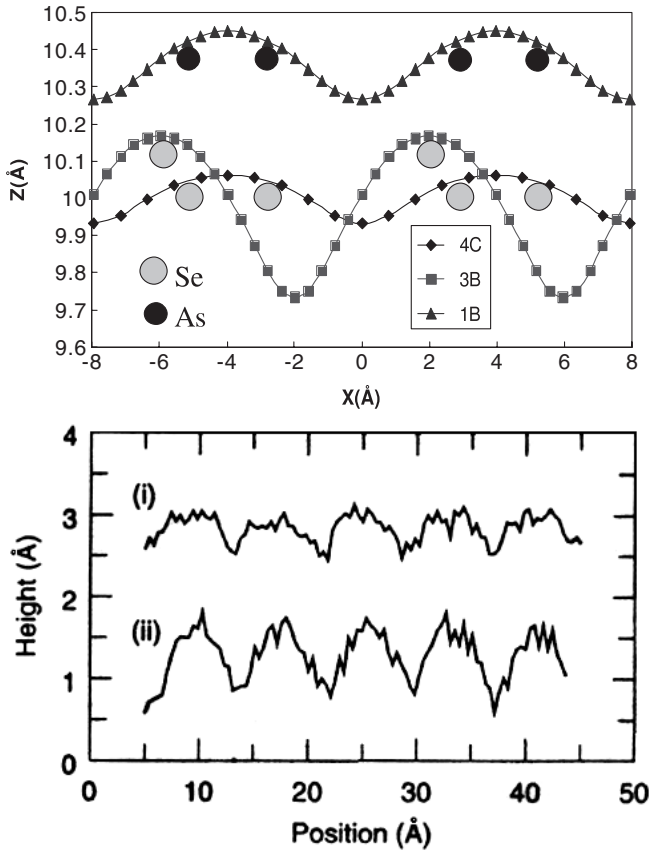

Figure 8. Top: theoretical surface topography along (■) the AA′ line in figure 7 for structure 3B, (▲) the line AA′ in figure 10 for structure 1B (shifted down rigidly by 0.4 Å to facilitate the comparison) and (♦) the Se dimers of the 4C structure. All the scales are in Å. The lateral position of the corresponding topmost atoms in each of the structures is indicated by circles (black for As, grey for Se). Bottom: experimental scans (taken from [18]) along the [1$\bar{1}$0] direction for (i) the GaAs(001)-2 × 4 surface and (ii) the GaAs(001):Se-(2 × 1).

reasonably well with the theoretical value of around 0.50 Å extracted from the corresponding line scan in our figure 8. Finally both the theoretical (our figure 9) and the experimental differential conductance (figure 2 in [18]) show a semiconductor gap completely free of states. Regarding this differential conductance, compare it with the LDOS shown in figure 6: the general behaviour of this curve is determined basically by the p_z density of states. Notice, in particular, that the p_x states give a negligible contribution to dI/dV due to the small coupling between the p_x-orbital and the tip.

In order to show that this good agreement is not just a coincidence, we have also analysed the STM currents and the surface topography of two other structures (1B and 4C) given in figure 1. Considering the 1B structure, we are trying to simulate the STM corrugation of the clean GaAs(001)-2 × 4 when we move the tip along the As dimers. Figure 10 shows the STM topography of the 1B structure, and we expect that the AA′ direction, along the As dimers, should show a corrugation very similar to the one measured by Pashley and Li [18] on the GaAs(001)-2 × 4, along similar As dimer directions. The calculated surface corrugation along the AA′ direction can be also found in figure 8. This curve should be compared with the curve (i) of figure 3(c) in [18]. Our calculated corrugation of 0.20 Å is slightly smaller than

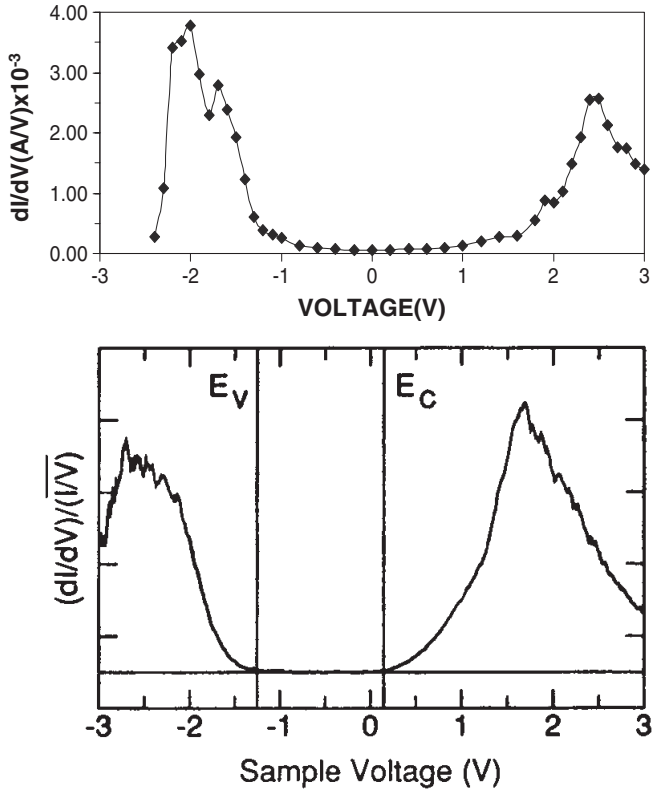

Figure 9. Top: theoretical differential conductance on top of a Se atom. The origin of the voltage corresponds to the position of the energy zero in figure 5. Bottom: experimental normalized conductance from a region of well-ordered GaAs(001):Se-(2 × 1) (taken from [18]).

the experimental corrugation of 0.35 Å, similar to what we found in the analysis of the 3B structure. Notice that absolute corrugation values are very sensitive to the tip configuration, not characterized in the experiments, but there is a remarkable agreement in the difference between the corrugation of the two structures in the theory (0.3 Å) and the experiment (0.35 Å).

Finally, we have also analysed the STM corrugation for the 4C structure of Pashley and Li, at the same conditions as previous cases, and moving the tip along the Se dimers of the surface. The surface corrugation for this case (shown in figure 8) appears to be less than 0.2 Å, smaller than the theoretical corrugation for the 1B structure (representing the As dimers in the clean reconstructed surface) and much less than the experimental data of Pashley and Li, confirming that the STM theoretical calculations do not support the 4C structure.

In conclusion, our STM theoretical simulations support the 3B model as the microscopic structure for the Se-passivated surface (as prepared by Pashley and Li [18]), showing that there is only a Se atom in the topmost layer, at variance with the Se dimers proposed by those authors.

6. Conclusions

All the theoretical and the experimental evidence presented in this paper tends to show that the structure in figure 2 represents the appropriate geometry of the Se-passivated GaAs(001)-2 × 1 reconstruction. Both DFT-LDA calculations (including the estimation of the surface

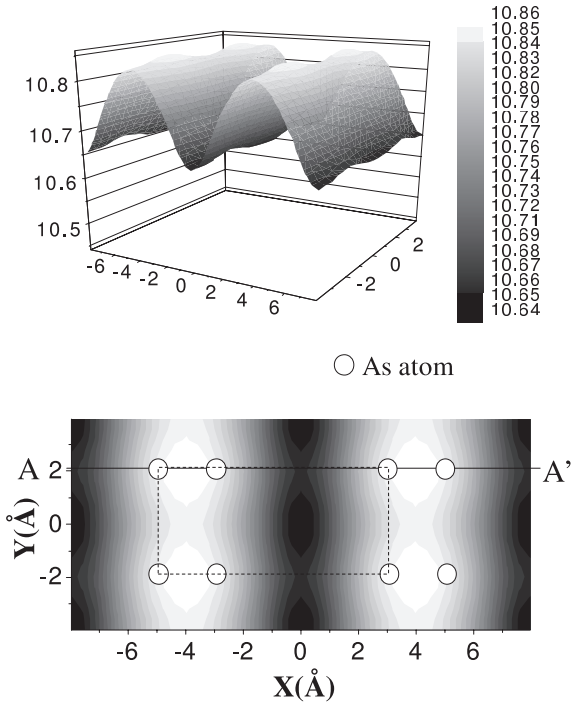

Figure 10. Topographical STM images (3 V, 0.1 nA) for the 1B structure in figure 1. X and Y correspond to the $[1\bar{1}0]$ and [110] crystallographic directions (see figure 1). The scales in the X, Y and Z directions are in Å. The reference point at $z = 0$ corresponds to the height of the topmost As atoms. The rectangle (dashed line) corresponds to the surface unit cell and white circles indicate the position of the As atoms. The spacing between the contour lines is 0.01 Å.

thermodynamic potentials) and STM images give a strong support to this structure, which is in agreement with the photoemission results presented in this paper, and the STM study of Pashley and Li [18].

The selenium modification of GaAs(001) in UHV is a reliable procedure for the preparation of well defined surfaces. The treatment results in gallium-selenide like layers. These surfaces are very unreactive and may be considered as chemically passivated. They resist considerable exposure to air and are already used as substrates for the growth of epitaxial films. However, in terms of an electronic passivation, the selenium modification is not successful. The band bending is reduced for n-type doped samples but increases for samples doped p-type. Therefore, surface states of donor and acceptor type exist in the band gap on these surfaces. Our theoretical results for the surface bands of the Se passivated GaAs(001) (see figure 5) suggest, however, that this surface should present a good passivation in terms of its electronic properties. We conclude that surface defects exist on the experimentally prepared Se-passivated GaAs(001) surfaces and that these defects may be related to doping atoms at the surface.

Acknowledgments

This work has been supported by the DIODE network (HPRN-CT-1999-00164) financed by the 5th Framework Programme of the European Commission. We also gratefully acknowledge the financial support of the Spanish CICYT under projects PB97–0028 and MAT2001-0665,

Comunidad de Madrid under contract 07N/0050/2001 and the German 'Bundesministerium für Bildung und Forschung' under grant no 05 622OCA 3. We thank D Westwood from the University of Wales for preparing the substrates and the BESSY staff for their help during the measurements.

References

[1] Flores F and Miranda R 1994 *Adv. Mater.* **6** 540
[2] Saiz-Pardo R, Pérez R, García-Vidal F J, Whittle R and Flores F 1999 *Surf. Sci.* **426** 26
[3] Kampen T U, Schmitsdorf R and Mönch W 1995 *Appl. Phys.* A **60** 391
[4] Hohenecker St, Kampen T U, Zahn D R T and Braun W 1998 *J. Vac. Sci. Technol.* B **16** 2317
[5] Hohenecker St, Kampen T U, Werninghaus T, Zahn D R T and Braun W 1999 *Appl. Surf. Sci.* **142** 28
[6] Mönch W *et al* 1995 *Proc. 22nd Int. Conf. on the Physics of Semiconductors* ed J Lockwood (Singapore: World Scientific)
[7] Weser T *et al* 1988 *Surf. Sci.* **201** 245
[8] Weser T, Ḃogen A, Konrad B, Schnell R D, Schug C A and Steinmann W 1987 *Phys. Rev.* B **35** 8184
[9] Krüger P and Pollman J 1990 *Phys. Rev. Lett.* **64** 1808
[10] Sandroff C J *et al* 1987 *Appl. Phys. Lett.* **51** 33
[11] Kamiyama S, Mori Y, Takahashi Y and Ohnaka K 1987 *Appl. Phys. Lett.* **58** 2595
[12] Howard A J, Ashby C I H, Lott J A, Schneider R P and Coreless R F 1996 *J. Vac. Sci. Technol.* A **12** 1063
[13] Bessolov V N, Lebedev M V, Shernyakov Y M and Tsarenkov B V 1997 *Mater. Sci. Eng.* B **44** 380
[14] Sandroff C J *et al* 1990 *J. Appl. Phys.* **67** 586
[15] Qiu J, Qian Q-D, Gunshor R L, Kobayashi M, Menke D R, Li D and Otsuka N 1990 *Appl. Phys. Lett.* **56** 1272
[16] Anderson G W, Hanf M C, Qin X R, Norton P R, Myrtle K and Heinrich B 1996 *Surf. Sci.* **346** 145
[17] Hahn Th, Metzner H, Plikat B and Seibt M 1998 *Appl. Phys. Lett.* **72** 2733
[18] Pashley M D and Li D 1994 *J. Vac. Sci. Technol.* A **12** 1848
[19] Li D and Pashley M D 1994 *Phys. Rev.* B **49** 13643
[20] Takatani S, Kikawa T and Nakzawa M 1992 *Phys. Rev.* B **45** 8498
[21] Pashley M D 1989 *Phys. Rev.* B **40** 10481
[22] Gundel S and Faschinger W 1999 *Phys. Rev.* B **59** 5602
[23] Shimada T, Ohuchi F S and Parkinson B A 1992 *J. Vac. Sci. Technol.* A **10** 539
[24] Joyce J J, Del Giudice M and Weaver J H 1989 *J. Electron. Spectrosc. Relat. Phenom.* **49** 31
[25] Cardona M and Ley L 1978 *Photoemission in Solids* (New York: Springer)
[26] Moriarty P, Murphy B, Roberts L, Cafolla A A, Hughes G, Koenders L and Bailey P 1994 *Phys. Rev.* B **50** 14237
[27] Larsen P K, Neave J H, van der Veen J F, Dobson P J and Joyce B A 1983 *Phys. Rev.* B **27** 4966
[28] Larive M, Jezequel G, Landesman J P, Solal F, Nagle J, Lepine B, Taleb-Ibrahimi A, Indlekofer G and Macadet X 1994 *Surf. Sci.* **304** 298
[29] Vitomirov I M, Raisanen A D, Finnefrock A C, Viturro R E, Brillson L J, Kirchner P D, Pettit G D and Woodall J M 1992 *J. Vac. Sci. Technol.* B **10** 1898
[30] Amokrane A, Sebenne C A, Cricenti A, Ottaviani C, Proix F and Eddrief M 1998 *Appl. Surf. Sci.* **123/124** 619
[31] LeLay G, Mao D, Kahn A, Hwu Y and Margaritondo G 1991 *Phys. Rev.* B **43** 14301
[32] Vitomirov I M, Raisanen A D, Finnefrock A C, Viturro R E, Brillson L J, Kirchner P D, Pettit G D and Woodall J M 1992 *J. Vac. Sci. Technol.* B **10** 1898
[33] Phillips J C 1984 *Phys. Rev.* B **30** 6195
[34] Lide D R (ed) 1994 *Handbook of Chemistry and Physics* 75th edn (Boca Raton, FL: CRC Press) pp 5–5
[35] Scimeca T, Watanabe Y, Berrigan R and Oshima M 1992 *Phys. Rev.* B **46** 10201
[36] Tsuchiya K, Sakakta M, Funyu A and Ikoma H 1995 *Japan. J. Appl. Phys.* **34** 5926
[37] Chambers S A and Sundaram V S 1990 *J. Vac. Sci. Technol.* B **9** 2342
[38] Märkl A, von der Emde M, Nowak C, Richter W and Zahn D R T 1995 *Surf. Sci.* **331–333** 631
[39] Biegelsen D K, Bringans R D, Nothrup J E and Swartz L-E 1994 *Phys. Rev.* B **94** 5424
[40] Maeda F, Watanabe Y, Scimeca T and Oshima M 1993 *Phys. Rev.* B **48** 4956
[41] Miwa S, Kimura K, Yasuda T, Kuo L H, Jin S, Tanaka K and Yao T 1996 *Appl. Surf. Sci.* **107** 184
[42] Lüth H 1993 *Surfaces and Interfaces of Solids* (*Springer Series in Surface Science* vol 15) 2nd edn (Berlin: Springer)
[43] Mönch W 1995 *Semiconductor Surfaces and Interfaces* (*Springer Series in Surface Science* vol 26) 3rd edn (Berlin: Springer)
[44] Demkov A A, Ortega J, Sankey O F and Grumbach M P 1995 *Phys. Rev.* B **52** 1618

[45] Bachelet G, Hamman D R and Schluter M 1982 *Phys. Rev.* B **26** 4199
[46] Perdew J P and Zunger A 1981 *Phys. Rev.* B **23** 5048
[47] Monkhorst H D and Pack J D 1976 *Phys. Rev.* B **13** 5188
[48] Ortega J, Perez R and Flores F 2000 *J. Phys.: Condens. Matter* **12** L21
[49] Ortega J 1998 *Comput. Mater. Sci.* **12** 192
[50] Mingo N *et al* 1996 *Phys. Rev.* B **54** 2225
[51] Jurczyszyn L, Ortega J, Pérez R and Flores F 2001 *Surf. Sci.* **482–485** 1350
[52] Martín-Moreno L and Vergés J A 1990 *Phys. Rev.* B **42** 7193
[53] Papaconstantopoulos D A 1986 *Handbook of the Band Structure of Elemental Solids* (New York: Plenum)
[54] Flores F, Martin-Rodero A, Goldberg E C and Duran J C 1988 *Nuovo Cimento* D **10** 303
[55] Blanco J M *et al* 2004 at press